Tissue-specific splicing of an *Ndufs6* gene-trap insertion generates a mitochondrial complex I deficiency-specific cardiomyopathy

Bi-Xia Ke[a,1], Salvatore Pepe[a,b,1], David R. Grubb[a,2], Jasper C. Komen[a], Adrienne Laskowski[a], Felicity A. Rodda[a,b], Belinda M. Hardman[a], James J. Pitt[a,b,c], Michael T. Ryan[d,e], Michael Lazarou[d,3], Jane Koleff[f], Michael M. H. Cheung[a,b,f], Joseph J. Smolich[a,b,4], and David R. Thorburn[a,b,c,4]

[a]Murdoch Childrens Research Institute, [c]Victorian Clinical Genetics Services Pathology and [f]Department of Cardiology, Royal Children's Hospital, Parkville, VIC 3052, Australia; [b]Department of Pediatrics, University of Melbourne, Melbourne, VIC 3010, Australia; and [d]Department of Biochemistry and [e]Australian Research Council Centre of Excellence for Coherent X-Ray Science, La Trobe University, Melbourne, VIC 3086, Australia

Edited by Jonathan G. Seidman, Harvard Medical School, Boston, MA, and approved February 28, 2012 (received for review August 26, 2011)

Mitochondrial complex I (CI) deficiency is the most common mitochondrial enzyme defect in humans. Treatment of mitochondrial disorders is currently inadequate, emphasizing the need for experimental models. In humans, mutations in the *NDUFS6* gene, encoding a CI subunit, cause severe CI deficiency and neonatal death. In this study, we generated a CI-deficient mouse model by knockdown of the *Ndufs6* gene using a gene-trap embryonic stem cell line. *Ndufs6*$^{gt/gt}$ mice have essentially complete knockout of the Ndufs6 subunit in heart, resulting in marked CI deficiency. Small amounts of wild-type *Ndufs6* mRNA are present in other tissues, apparently due to tissue-specific mRNA splicing, resulting in milder CI defects. *Ndufs6*$^{gt/gt}$ mice are born healthy, attain normal weight and maturity, and are fertile. However, after 4 mo in males and 8 mo in females, *Ndufs6*$^{gt/gt}$ mice are at increased risk of cardiac failure and death. Before overt heart failure, *Ndufs6*$^{gt/gt}$ hearts show decreased ATP synthesis, accumulation of hydroxyacylcarnitine, but not reactive oxygen species (ROS). *Ndufs6*$^{gt/gt}$ mice develop biventricular enlargement by 1 mo, most pronounced in males, with scattered fibrosis and abnormal mitochondrial but normal myofibrillar ultrastructure. *Ndufs6*$^{gt/gt}$ isolated working heart preparations show markedly reduced left ventricular systolic function, cardiac output, and functional work capacity. This reduced energetic and functional capacity is consistent with a known susceptibility of individuals with mitochondrial cardiomyopathy to metabolic crises precipitated by stresses. This model of CI deficiency will facilitate studies of pathogenesis, modifier genes, and testing of therapeutic approaches.

mouse model | mitochondrial diseases

Mitochondria generate the majority of energy required for cellular function and survival. Defects in mitochondrial oxidative phosphorylation (OXPHOS) cause a wide range of diseases, collectively affecting ~1/5,000 births (1). OXPHOS dysfunction was first identified in neuromuscular disorders but symptoms can potentially affect any organ, with any age of onset and any mode of inheritance (2). The heart, being highly energy dependent, is particularly vulnerable to OXPHOS defects, with cardiac involvement recognized in about a third of children and up to 80% of adults with OXPHOS disorders (3, 4). Complex I (CI) deficiency is the most common OXPHOS disorder and has a wide range of clinical presentations, including neurodegeneration, muscle weakness, cardiac failure, liver failure, and early death, often in childhood (5, 6). As identified by Cochrane review, "there is currently no clear evidence supporting the use of any intervention in OXPHOS disorders" (7). Thus, there is an urgent need for suitable animal models to study pathogenic mechanisms and novel therapeutic approaches. Such models can also shed light on the wide range of common, complex diseases to which mitochondrial dysfunction contributes (8).

Despite the high prevalence of OXPHOS disorders, relatively few genetic models have been developed. Until recently, the only mouse model of CI deficiency exhibited decreased expression of apoptosis-inducing factor (AIF), a mitochondrial protein first identified as a cell death mediator (9–11). AIF is also thought to be involved in the assembly and/or stabilization of CI (12), but the highly variable symptoms in individual AIF mice and the role of AIF in cell death complicate interpretation of the pathogenesis and potentially the treatment response in AIF mouse models. A recent report of patients with pathogenic *AIF* mutations found no evidence of CI deficiency (13), further complicating its role in CI biogenesis in humans.

It is desirable to have "pure" mouse models of CI deficiency to investigate pathogenic mechanisms and trial novel treatment approaches. Fourteen of the 45 CI subunits are highly conserved across species and represent core subunits (14), whereas the 31 supernumerary subunits were gained at different evolutionary stages. Analysis of mutations in CI patients suggests that knockouts of the 7 nuclear-encoded core subunit genes are likely to be embryonic lethal (15). Recently, the first CI subunit knockout model was generated by knocking out the *Ndufs4* gene, which is in the third most conserved group of CI subunits (14). Patients with *NDUFS4* mutations typically have two null-type mutations and develop the neurodegenerative condition, Leigh syndrome (15). *Ndufs4* knockout mice develop encephalomyopathy and die within 7 wk (16). A brain-specific *Ndufs4* knockout showed a nearly identical phenotype to the systemic knockout with death by 7 wk (17). These are useful models but do not develop the characteristic neuropathology of Leigh syndrome and the early lethality means they can only be used in short-term treatment studies.

We and others have described children with mutations in the *NDUFS6* subunit gene (18, 19), all of whom died in the first month of life. The *NDUFS6* gene is in the second most conserved

Author contributions: B.-X.K., S.P., D.R.G., J.J.S., and D.R.T. designed research; B.-X.K., S.P., D.R.G., J.C.K., A.L., F.A.R., B.M.H., J.J.P., M.L., J.K., M.M.H.C., and J.J.S. performed research; B.-X.K., S.P., D.R.G., J.C.K., A.L., F.A.R., B.M.H., J.J.P., M.T.R., M.L., J.K., M.M.H.C., J.J.S., and D.R.T. analyzed data; and B.-X.K., S.P., J.C.K., A.L., J.J.P., M.T.R., M.M.H.C., J.J.S., and D.R.T. wrote the paper.

The authors declare no conflict of interest.

This article is a PNAS Direct Submission.

[1]B.-X.K and S.P. contributed equally to this work.

[2]Present address: Baker International Diabetes Institute, Heart and Diabetes Institute, Melbourne, VIC 3004, Australia.

[3]Present address: Biochemistry Section, Surgical Neurology Branch, National Institute of Neurological Disorders and Stroke, National Institutes of Health, Bethesda, MD 20892.

[4]To whom correspondence may be addressed. E-mail: david.thorburn@mcri.edu.au or joe.smolich@mcri.edu.au.

This article contains supporting information online at www.pnas.org/lookup/suppl/doi:10.1073/pnas.1113987109/-/DCSupplemental.

group of CI subunit genes (14) and all patients had null-type mutations. The aim of the present study was to generate and characterize a CI-deficient mouse model by knockdown of the *Ndufs6* gene using gene-trap embryonic stem cell (ESC) lines (20). *Ndufs6*$^{gt/gt}$ mice have reduced expression of the Ndufs6 subunit resulting in different degrees of CI deficiency in various tissues, but most pronounced in the heart. The resultant cardiomyopathy has a markedly diminished functional capacity and a predisposition to heart failure.

Results

Generation of *Ndufs6*$^{gt/gt}$ Mice. *Ndufs6*$^{gt/gt}$ mice were generated by knockdown of the *Ndufs6* gene using gene-trap ESC lines (20). The mutagenesis vector generates a fusion protein between the N terminus of *Ndufs6* and a β-galactosidase–neomycin resistance (β-GEO) cassette (Fig. S1*A*). Immunocytochemical staining shows mitochondrial localization of fusion protein in *Ndufs6*$^{+/gt}$ ESC (Fig. S1*B*) and SDS/PAGE immunoblotting confirms expression of fusion protein (Fig. S1*C*). Blue native polyacrylamide gel electrophoresis (BN-PAGE) immunoblotting of mitochondria demonstrates that the fusion protein migrates at the expected size for the tetramer (~550 kDa) and is not assembled into CI (Fig. S1*D*). Mice heterozygous for the mutation were generated on a mixed 129/Ola and C57BL/6 background using standard methods of host embryo microinjection, chimera production, and germ-line transmission (21).

Phenotype of *Ndufs6*$^{gt/gt}$ Mice. At 4 wk of age, offspring of heterozygous parents were present in an ~1:2:1 Mendelian ratio (91 wild-type, 168 heterozygous, and 91 homozygous, $\chi^2 = 0.56$, $P > 0.7$), indicating that no fetal loss was caused by the gene-trap insertion. Both male and female *Ndufs6*$^{gt/gt}$ mice were fertile. However, *Ndufs6*$^{gt/gt}$ females produced smaller litters and pups had a lower neonatal survival rate compared with offspring from unaffected females (Fig. S2*A*). For the first 4 mo of life, *Ndufs6*$^{gt/gt}$ mice had an apparently normal general phenotype, with normal weight gain (Fig. S2*B*). However, from 4 mo in males and 8 mo in females, *Ndufs6*$^{gt/gt}$ mice were prone to rapid onset weight loss and sudden death. For ethical reasons, mice over these ages were therefore killed when they lost >20% of their maximum weight. Long-term survival in *Ndufs6*$^{gt/gt}$ males was about half that of females (Fig. S3).

From as early as 30 d of age, cardiac enlargement was evident in *Ndufs6*$^{gt/gt}$ mice and more pronounced in males, with a near-doubling of heart weight (Fig. 1*A*) and the heart-to-body weight ratio (Fig. 1*B*), associated with increased myocardial mRNA expression of *Anp* (atrial natriuretic peptide), but not β-*MHC* (beta myosin heavy chain) (Fig. 1*C*). However, cardiac enlargement was more severe in mice with weight loss, particularly males, with heart weight 3.2-fold and the heart-to-body weight ratio 3.9-fold that of wild-type mice, accompanied by pronounced up-regulation of myocardial *Anp* and β-*MHC* mRNA expression (Fig. 1). The combined left and right atrial weight in *Ndufs6*$^{gt/gt}$ with weight loss (31.7 ± 5.2 mg) also exceeded that in wild-type (6.3 ± 0.7 mg) or *Ndufs6*$^{gt/gt}$ without weight loss (8.2 ± 1.0 mg; $P < 0.001$). This constellation of findings was consistent with the onset of overt cardiac failure in mice with weight loss. Because cardiac enlargement in *Ndufs6*$^{gt/gt}$ mice was more prominent in males, and cardiac failure may produce potentially confounding effects on myocardial energetics and ultrastructure, we focus on the phenotype of male mice without failure in the next sections.

CI Deficiency. *Ndufs6*$^{gt/gt}$ mice had a partial knockdown of the *Ndufs6* gene, with small amounts of wild-type mRNA (between 1 and 34%) detected in all tissues studied (Fig. 2*A*). This resulted in reduced expression of Ndufs6 protein in various tissues, especially the heart (Fig. 2*B*). CI activity was also decreased most markedly in heart, representing ~10% of normal CI activity (Fig. 2*C*). BN-PAGE immunoblotting showed a reduced amount of fully assembled CI in various tissues (Fig. 2*D*), presumably due to the decrease in Ndufs6 protein. *Ndufs6*$^{gt/gt}$ mice had an isolated CI defect as the cardiac activities of OXPHOS complexes II, III, and IV (CII, CIII, and CIV) were normal (Fig. 3*A*). Isolated heart mitochondria from *Ndufs6*$^{gt/gt}$ mice showed a decreased capacity to generate ATP from substrates oxidized via CI but not via CII (Fig. 3*B*).

To examine whether fatty acid metabolism was affected by CI deficiency, acylcarnitine levels were measured in mouse hearts. *Ndufs6*$^{gt/gt}$ mouse hearts showed a general increase in hydroxyacylcarnitines with chain length C6 to C18, with significantly greater levels of OHC6 and OHC8 than wild-type (Fig. 3*C*). However, reactive oxygen species (ROS) production by isolated heart mitochondria did not differ between *Ndufs6*$^{gt/gt}$ and wild-type (Fig. 3*D*).

Cardiac Morphology and Echocardiography. In fixed hearts sectioned transversely at ventricular midcavity level, *Ndufs6*$^{gt/gt}$ mice showed increases in chamber dimensions and wall thickness (Fig. 4*A*), plus higher left and right ventricular free wall and septal weights (Fig. 4*B*). Furthermore, left ventricular end-systolic and end-diastolic diameters and posterior wall thickness were increased, and fractional shortening reduced in *Ndufs6*$^{gt/gt}$ mice on echocardiography (Fig. 4*C* and Table 1).

Myocardial Ultrastructure. Compared with wild-type mice (Fig. 5*A*), left ventricular myocardium of *Ndufs6*$^{gt/gt}$ mice showed scattered areas of fibrosis (Fig. 5*B*), but the ultrastructure of myofibers and nuclei appeared normal on transmission electron microscopy (Fig. 5 *C* and *D*). However, compared with wild-type mice (Fig. 5*E*), mitochondrial morphology was abnormal in *Ndufs6*$^{gt/gt}$ mice, with the central area frequently denser than the periphery (Fig. 5*F*), due to narrowing of both the matrix

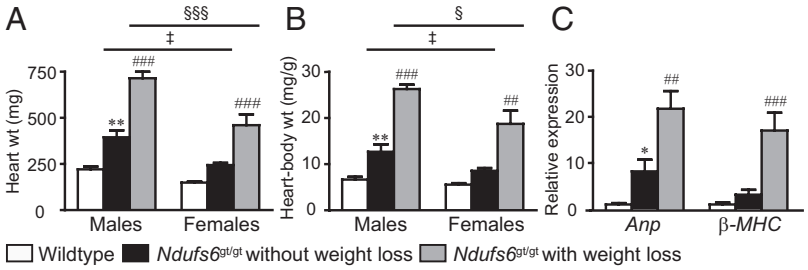

Fig. 1. Cardiac enlargement. (*A*) Wet whole heart weight and (*B*) heart-to-body weight ratio in wild-type mice and in *Ndufs6*$^{gt/gt}$ mice with or without weight loss; n = 9–15 per subgroup. (*C*) Myocardial mRNA expression of *Anp* and β-*MHC*; n = 3–9 per subgroup. $^{*}P < 0.05$, $^{**}P < 0.01$, wild-type vs. *Ndufs6*$^{gt/gt}$ mice without weight loss; $^{\#\#}P < 0.01$, $^{\#\#\#}P < 0.001$, *Ndufs6*$^{gt/gt}$ mice with vs. without weight loss; $^{\ddagger}P < 0.05$, male vs. female *Ndufs6*$^{gt/gt}$ mice without weight loss; $^{\S}P < 0.05$, $^{\S\S\S}P < 0.001$, male vs. female *Ndufs6*$^{gt/gt}$ mice with weight loss. Wt, weight.

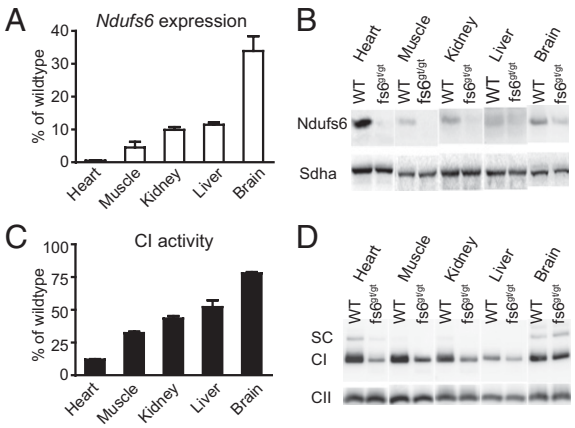

Fig. 2. Ndufs6 expression and CI deficiency. (*A*) Wild-type (WT) *Ndufs6* mRNA levels measured by quantitative real-time PCR in tissues of male *Ndufs6*$^{gt/gt}$ mice (4 mo). Results are expressed as percentage of wild-type levels. (*B*) SDS/PAGE immunoblotting to detect Ndufs6 protein expression in isolated mitochondria of the same tissues. The CII 70-kDa subunit (Sdha) was used as loading control. (*C*) CI activity in tissues of male *Ndufs6*$^{gt/gt}$ mice (4 mo). Results are expressed as percentage of wild-type levels relative to citrate synthase. (*D*) BN-PAGE immunoblotting to detect the amounts of fully assembled CI in the mitochondria of the same tissues. Level of fully assembled CII was used as loading control. fs6, *Ndufs6*; SC, supercomplex.

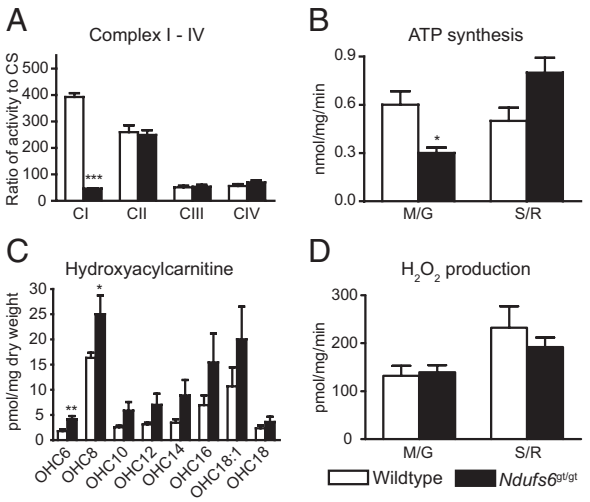

Fig. 3. Mitochondrial functional parameters. (*A*) Activity of complexes I–IV in mouse heart, expressed relative to citrate synthase (CS) activity; n = 6–8. (*B*) ATP synthesis rates in isolated heart mitochondria via substrates oxidized by CI (M/G, malate and glutamate) versus substrates oxidized via CII (S/R, succinate and rotenone); n = 4. (*C*) Heart hydroxyacylcarnitine levels; n = 8. (*D*) H_2O_2 production in isolated heart mitochondria; n = 4. All mice were 4-mo-old males. $^*P < 0.05$, $^{**}P < 0.01$, $^{***}P < 0.001$; wild-type vs. *Ndufs6*$^{gt/gt}$ mice. Data expressed as mean ± SEM.

(6.3 ± 0.2 vs. 19.8 ± 0.5 nm; $P < 0.001$) and intercristal spaces (7.8 ± 0.2 vs. 15.5 ± 0.4 nm; $P < 0.001$). In association with this altered morphology, mitochondrial area in *Ndufs6*$^{gt/gt}$ mice (0.62 ± 0.03 μm^2) was smaller than in wild-type mice (0.82 ± 0.06 μm^2; $P < 0.01$).

Isolated Heart Function. At the baseline preload, left ventricular peak systolic pressure was ∼12 mmHg lower and end-diastolic pressure ∼7 mmHg higher in *Ndufs6*$^{gt/gt}$ mice, whereas aortic output, coronary flow, and left ventricular stroke volume, contractility (+δP/δT) and relaxation (−δP/δT) were 40–60% lower than in wild-type mice. These differences were sustained when left atrial filling pressure was systematically varied between 5 and 25 mmHg to define the Frank-Starling relationship (Table S1). Notably, with increased left atrial filling, resultant demand-induced increases in cardiac output (Fig. 6*A*) and external work (Fig. 6*B*) were markedly attenuated in *Ndufs6*$^{gt/gt}$ mice. Furthermore, *Ndufs6*$^{gt/gt}$ hearts were situated at the lower end of a highly linear stroke volume–external work relationship (Fig. 6*C*).

Discussion

In this study, we generated a mouse model of mitochondrial CI deficiency, in which insertion of a gene-trap vector disrupted expression of the *Ndufs6* gene, leading to decreased levels of Ndufs6 protein. *Ndufs6*$^{gt/gt}$ mice had primarily a cardiac phenotype, manifested as a cardiomyopathy associated with a doubling of heart weight, impaired systolic function, and a reduction in functional capacity. Males were most severely affected, with a propensity to develop cardiac failure and diminished survival after 4 mo of age.

In *Ndufs6*$^{gt/gt}$ mice, the amount of intact CI and CI activity were decreased in all tissues tested but, similar to *NDUFS6* patients (18), CII, CIII, and CIV activities were unaffected. However, residual CI activity showed an unexpected tissue variation, with CI activity lowest in heart, at ∼10% of the wild-type value. Levels of wild-type *Ndufs6* mRNA were low in *Ndufs6*$^{gt/gt}$ mice but, surprisingly, appreciable residual amounts of wild-type mRNA were present in tissues such as brain, a finding which contrasts with the apparent systemic CI defect seen in patients with *NDUFS6* mutations (18). The likely mechanism for this tissue variability is that some wild-type mRNA is formed by splicing over the gene-trap vector sequence. The virtual absence of wild-type mRNA in *Ndufs6*$^{gt/gt}$ hearts and the severe cardiac phenotype suggest that such splicing occurs in brain, but not heart. Analysis of midgestation *Ndufs6*$^{gt/gt}$ mouse embryos showed low levels of wild-type *Ndufs6* mRNA in both heart and brain (Fig. S4). However, as development proceeds, it appears that the extent of tissue-specific splicing may increase in some tissues, but not others. We are not aware of splicing over the gene-trap vector sequence being described previously in gene-trap mice, but tissue-specific splicing codes are starting to be identified (22). Importantly, whereas cardiac muscle has a high energy requirement and is dependent on OXPHOS for normal function, the cardiac specificity of the *Ndufs6*$^{gt/gt}$ phenotype is unlikely to be due simply to high reliance on CI activity or different energy substrate preferences in heart. In a mouse model of systemic CI deficiency (i.e., *Ndufs4*$^{-/-}$ mice), animals die from neurological disease without overt heart disease (16, 17).

In *Ndufs6*$^{gt/gt}$ mice, we did not observe the crippled CI species seen in the fibroblasts of *NDUFS6* patients (18). This could be due to the partially assembled CI species in the tissues of *Ndufs6*$^{gt/gt}$ mice being less stable than those in patient fibroblasts and thus becoming undetectable after mitochondrial isolation or because tissues dense with mitochondria and reliant on high rates of OXPHOS (such as heart) have more rapid clearance of partially assembled CI. Alternatively, the lack of this assembly intermediate in our model may suggest that Ndufs6 plays a somewhat different role in the assembly or stability of CI in mice and humans. We note that the Ndufs6–βGEO fusion protein is stable in heterozygous ESC (Fig. S1*C*) and in heterozygous and homozygous mutant hearts (Fig. S5). However, the presence of the fusion protein does not appear to contribute to pathogenicity as it is not incorporated into assembled CI (Fig. S1*D*), and heterozygous mice lack any detectable phenotype.

The decreased CI activity in *Ndufs6*$^{gt/gt}$ hearts resulted in a decreased rate of mitochondrial ATP synthesis with CI substrates but no apparent increase in ROS generation. A general increase in hydroxyacylcarnitines with chain length of C6 to C18

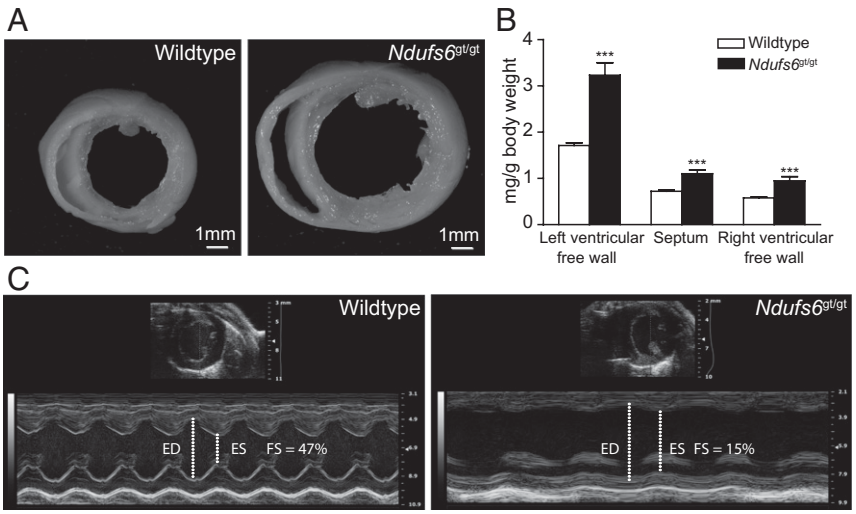

Fig. 4. Cardiac phenotype. (*A*) Cross-sections of perfusion-fixed hearts from wild-type and *Ndufs6*$^{gt/gt}$ male mice. (*B*) Regional heart weights of male wild-type and *Ndufs6*$^{gt/gt}$ mice. ***$P < 0.001$, wild-type vs. *Ndufs6*$^{gt/gt}$. (*C*) M-mode echocardiographic images of left ventricle obtained with the Vevo 2100 system in wild-type and *Ndufs6*$^{gt/gt}$ male mice. ED, end-diastolic diameter; ES, end-systolic diameter; FS, fractional shortening.

was observed in *Ndufs6*$^{gt/gt}$ hearts (Fig. 3*C*), presumably due to an increased mitochondrial NADH/NAD$^+$ ratio inhibiting the NAD$^+$-dependent oxidation of 3-hydroxy fatty acyl-CoA species in the β-oxidation spiral.

Male *Ndufs6*$^{gt/gt}$ mice showed a more severe phenotype than females in regard to cardiac enlargement, propensity to develop cardiac failure, and survival rate. Sex differences with OXPHOS defects have also been reported in mouse models of mitochondrial disease affecting the assembly of CIV. Thus, in Sco2 mutant mice, males have earlier onset of muscle weakness (23), whereas in muscle-specific Cox10 knockout mice, females have a more beneficial response to up-regulation of the PGC-1α pathway (24). Furthermore, in human mitochondrial disease, typically more male patients are affected (male/female ratio: 1.5:1) (3). It is also well documented that male mice in a range of nonmitochondrial models of cardiac disease often show more severe phenotypes in parameters such as cardiac hypertrophy, cardiac fibrosis, and survival (25). These sex-related differences are presumably related to a sex hormone effect, as estradiol has been reported to stimulate mitochondrial biogenesis (26), whereas androgens appear to promote cardiac enlargement and fibrosis (27).

In male *Ndufs6*$^{gt/gt}$ mice, occurrence of heart failure and sudden death spanned a relatively wide time interval (Fig. S3). This variability could be a stochastic process or due to environmental modifiers, although the latter seems unlikely as mice were housed with minimal variation in diet, temperature, and pathogen exposure. Whether variability is influenced by one or more modifier genes that segregate in the mixed genetic background could be tested in future gene mapping studies using *Ndufs6*$^{gt/gt}$ mice bred on different genetic backgrounds.

Echocardiographic and isolated heart studies indicated that resting systolic function was substantially impaired even in *Ndufs6*$^{gt/gt}$ mice without cardiac failure. This impairment was particularly striking, given that myocardial ultrastructural changes

Table 1. Left ventricular wall thickness, chamber dimensions, and fractional shortening in wild-type and *Ndufs6*$^{gt/gt}$ male mice of similar age

	Wild type (n = 9)	*Ndufs6*$^{gt/gt}$ (n = 6)	P
PWT, mm	0.85 ± 0.04	1.08 ± 0.07	<0.01
ED, mm	3.67 ± 0.14	4.58 ± 0.29	<0.01
ES, mm	2.19 ± 0.12	3.84 ± 0.33	<0.001
FS, %	40 ± 1	16 ± 3	<0.001
Age, wk	11.4 ± 1.9	9.3 ± 2.2	0.5

Data are presented as mean ± SEM. ED, end-diastolic diameter; ES, end-systolic diameter; FS, fractional shortening; PWT, end-diastolic posterior wall thickness.

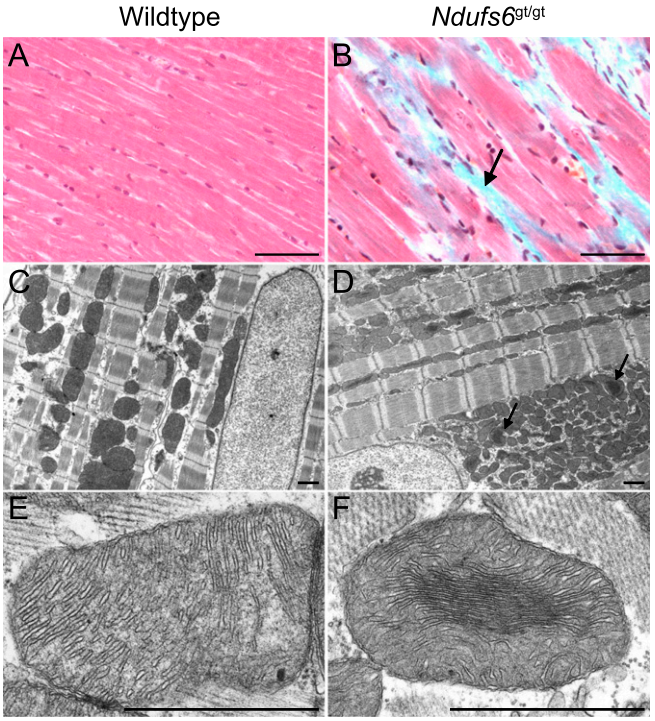

Fig. 5. Myocardial ultrastructure. Masson's trichrome staining of cardiac muscle in wild-type mice (*A*) and *Ndufs6*$^{gt/gt}$ mice (*B*), showing fibrosis in the latter as blue staining (arrow). Ultrastructure of myofibers and the nucleus are normal in left ventricular myocardium of wild-type mice (*C*) and *Ndufs6*$^{gt/gt}$ mice (*D*), but mitochondria in the latter contain central dense areas (arrows). Compared with wild-type mice (*E*), higher power reveals that myocardial mitochondria of *Ndufs*$^{gt/gt}$ mice have tightly packed central cristae with diminished matrix space (*F*). [Scale bars, 0.1 mm (*A* and *B*); 1 μm (*C*–*F*)].

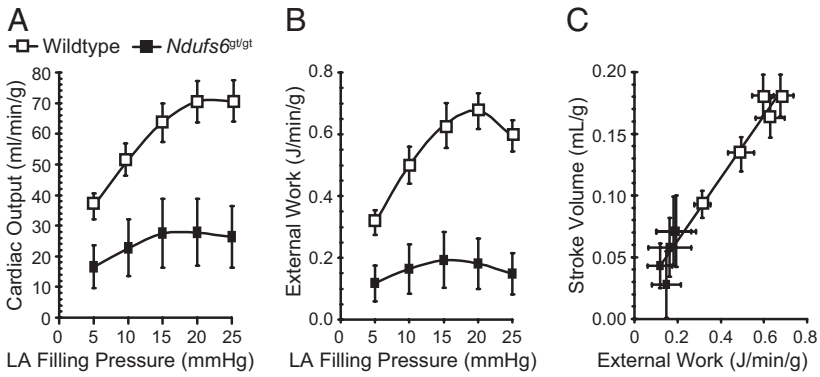

Fig. 6. Isolated heart studies. Increases in left atrial filling pressure resulted in augmented cardiac output (*A*), external work (*B*), and a close correlation ($r^2 = 0.96$; $y = 0.25\times + 0.01$) between stroke volume and external work (*C*). However, *Ndufs6*$^{gt/gt}$ mice had lower cardiac output and external work responses than wild-type mice ($P < 0.01$ at each preload level).

appeared to be restricted to scattered fibrosis and smaller mitochondria with abnormal morphology. Furthermore, the inability of hearts from *Ndufs6*$^{gt/gt}$ mice to increase external work in response to increased filling demonstrated that *Ndufs6* deficiency-induced cardiomyopathy markedly limited Frank-Starling properties and reduced functional work capacity. Thus, *Ndufs6*$^{gt/gt}$ mice are anticipated to be vulnerable to energy deficits and myocardial injury during conditions of high work stress or ischemia reperfusion. This is consistent with the observation that patients with mitochondrial cardiomyopathy often have prolonged periods of clinical stability but are susceptible to acute metabolic decompensation precipitated by fasting, infection, or other stresses (28, 29). This metabolic fragility is also seen in OXPHOS disorders affecting other tissues. For example, brain magnetic resonance imaging studies in patients with OXPHOS disorders indicated a decline in phosphorylation potential, implying a similar low energy reserve (30) to that seen in *Ndufs6*$^{gt/gt}$ mouse hearts. These observations emphasize that prevention or minimizing the impact of metabolic stresses is a key approach to maintaining the stability of patients with OXPHOS disorders.

Although *Ndufs6*$^{gt/gt}$ mice resembled many of the biochemical, morphological, and functional features of human patients, they did not recapitulate all of them. Compared with *NDUFS6* patients who die within the first week of life, *Ndufs6*$^{gt/gt}$ mice can survive for more than 4 mo, presumably because the CI deficiency is heart specific rather than systemic, and cardiac adaptation may be possible until reserve capacity is ultimately lost. All *NDUFS6* patients (except one) diagnosed so far did not have a specific cardiac assessment due to the system-wide severity of the disease causing early death (18, 19). Hence, cardiac involvement in these patients cannot be excluded. Indeed, we recently showed that cardiac problems are present in one-third of children with OXPHOS disorders, with boys affected more than girls (3). *Ndufs6*$^{gt/gt}$ mice will be a useful model to study the pathogenesis induced by mitochondrial cardiomyopathy and potentially for the identification of modifier genes and for testing therapeutic approaches, because these mice have a relatively longer lifespan than *NDUFS6* patients.

Methods

Generation of Gene-Trap (*Ndufs6*$^{gt/gt}$) Mice. The AR01380 ESC line was purchased from the International Gene Trap Consortium (www.genetrap.org). *Ndufs6*$^{gt/gt}$ mice were generated at the Transgenic Animal Service of Queensland (Brisbane, Australia) using standard methods. Mice were bred and maintained following an approved protocol by the Murdoch Childrens Research Institute (MCRI) Animal Ethics Committee. Details are in *SI Methods*.

Immunocytochemistry, Collagen Staining, and EM. To assess the mitochondrial localization of fusion protein, gene-trap ESC were stained with either mouse anti–β-Gal monoclonal antibody (1:200; Promega) followed by antimouse IgG Alexa 488 (1:200; Molecular Probes) or rabbit anti-MnSOD polyclonal antibody (1:400; Assay Designs) followed by antirabbit IgG Alexa 546 (1:400; Molecular Probes). Details are in *SI Methods*. To visualize interstitial collagen deposition, hearts were immersion fixed with 10% (wt/vol) formalin (Sigma) for 24 h, with 4 μM paraffin sections, then stained with Masson's trichrome stain (Sigma). For electron microscopy, hearts were perfusion fixed with 2.5% (vol/vol) glutaraldehyde and 4% (wt/vol) paraformaldehyde in 0.1 M sodium cacodylate buffer (pH 7.4), then immersed in the same fixative for 24–48 h at 4 °C. Tissue blocks were excised from the left ventricular free wall and prepared using standard procedures, as previously described (31, 32).

Mitochondrial Morphometry. Mitochondrial quantitation was performed on transmission electron micrographs from two wild-type and two *Ndufs6*$^{gt/gt}$ mice using Image J software (National Institutes of Health). The mitochondrial area was measured at low power (4,900×) in mitochondria situated adjacent to longitudinally sectioned myofibrils. Widths of the matrix and intercristal space in central and peripheral regions of mitochondria from *Ndufs6*$^{gt/gt}$ mice were measured at higher power (27,500×) in mitochondria with parallel cristae. Between 59 and 149 measurements were acquired per variable.

Longevity Study. Mice were monitored up to 1 y. Details are in *SI Methods*.

Enzyme Activity Assay. Mouse tissues were homogenized and assays performed on postnuclear supernatants as described previously (5), except that assay temperatures were 25 °C.

Mitochondrial Isolation. Mice (4 and 17–21 mo) were killed by cervical dislocation and tissues collected for mitochondrial isolation. Mitochondria were isolated from tissues (except brain) as previously described (33). Brain mitochondria were isolated as per Sims et al. (34), except digitonin was decreased to 3.1 mg/g initial wet brain weight. Protein concentrations were measured using BCA (Sigma) (35).

Western and Blue-Native PAGE Blot. Western blot analysis was similar to the protocol of Calvo et al. with minor modifications (36), using a rabbit polyclonal Ndufs6 antibody. BN-PAGE was performed on isolated mitochondria from various tissues as previously described (37), using a rabbit polyclonal antibody to the CI 39-kDa subunit. Details are in *SI Methods*.

Acylcarnitine Measurement. Acylcarnitine species were analyzed from ~10 mg of heart tissue using an electrospray tandem mass spectrometry approach. Details are in *SI Methods*.

RNA Isolation and Quantitative PCR Analysis. Details are in *SI Methods*.

Mitochondrial Functional Assays. Myocardial ATP synthesis assay was performed on freshly isolated mitochondria (6.25 μg/mL) incubated with either 10 mM malate and 10 mM glutamate (CI substrate), or 10 mM succinate and 5 μM rotenone (CII substrate) as described previously (5), but without the of digitonin treatment. ATP concentrations were measured with the ATP Bioluminescence CLSII kit (Roche Diagnostics) using a FLUOstar OPTIMA

GENETICS

microplate reader (BMG Labtechnologies). ROS production (H_2O_2) in live mitochondria (25 μg/mL) was assessed using the fluorescent probe Amplex Red via the protocol of Morten et al. with minor modifications (38). H_2O_2 production was measured fluorometrically (excitation 540 nm, emission 590 nm) over a 20-min period on a FLUOstar OPTIMA microplate reader.

Echocardiography. Echocardiography was performed on anesthetized mice using a 12-MHz phased array transducer and Vivid I ultrasound machine (GE Medical Systems) or a 40-MHz linear array transducer and Vevo 2100 ultrasound system (VisualSonics). Details are in *SI Methods*.

Cardiac Function. Isolated working heart studies were performed to exclude neural and humoral influences and to control heart rate, preload, and afterload. The heart-to-body weight ratio of *Ndufs6*$^{gt/gt}$ mice in these studies was almost double that of wild-type mice (11.4 ± 1.5 vs. 6.5 ± 0.3 mg/g; P = 0.005). Left ventricular Frank-Starling relationships were measured over a left atrial filling pressure range of 5–25 mmHg, as previously described (39). Details are in *SI Methods*.

Statistics. Data were analyzed using GraphPad Prism 4. Differences were considered significant at $P < 0.05$. Data between two groups were compared with an unpaired T test. Data from more than two groups were evaluated with one-way ANOVA followed by Tukey's post hoc analysis. A log-rank test was used for Kaplan-Meier survival analysis. All data are presented as mean ± SEM.

ACKNOWLEDGMENTS. We thank Andrew Heinmiller for assistance with the acquisition of Vevo 2100 echocardiographic images and the staff from Murdoch Childrens Research Institute's animal facility, Victorian Clinical Genetics Services Pathology Newborn Screening Laboratory, Transgenic Animal Service of Queensland, Royal Children's Hospital Department of Anatomical Pathology, University of Melbourne Electron Microscopy Unit, and Florey Neuroscience Institute Integrative Neuroscience Facility for excellent technical support. This work was supported by grants and a Principal Research Fellowship from the Australian National Health and Medical Research Council (to D.R.T.), the Muscular Dystrophy Association, the SMILE Foundation, the Jenour Foundation, the Financial Markets Foundation for Children, and the Victorian Government's Operational Infrastructure Support Program.

1. Skladal D, Halliday J, Thorburn DR (2003) Minimum birth prevalence of mitochondrial respiratory chain disorders in children. *Brain* 126:1905–1912.
2. Pagliarini DJ, et al. (2008) A mitochondrial protein compendium elucidates complex I disease biology. *Cell* 134:112–123.
3. Yaplito-Lee J, et al. (2007) Cardiac manifestations in oxidative phosphorylation disorders of childhood. *J Pediatr* 150:407–411.
4. Limongelli G, et al. (2010) Prevalence and natural history of heart disease in adults with primary mitochondrial respiratory chain disease. *Eur J Heart Fail* 12:114–121.
5. Kirby DM, et al. (1999) Respiratory chain complex I deficiency: An underdiagnosed energy generation disorder. *Neurology* 52:1255–1264.
6. Loeffen JL, et al. (2000) Isolated complex I deficiency in children: Clinical, biochemical and genetic aspects. *Hum Mutat* 15:123–134.
7. Chinnery P, Majamaa K, Turnbull D, Thorburn D (2006) Treatment for mitochondrial disorders. *Cochrane Database Syst Rev*(1):CD004426.
8. Wallace DC, Fan W (2009) The pathophysiology of mitochondrial disease as modeled in the mouse. *Genes Dev* 23:1714–1736.
9. Joza N, et al. (2005) Muscle-specific loss of apoptosis-inducing factor leads to mitochondrial dysfunction, skeletal muscle atrophy, and dilated cardiomyopathy. *Mol Cell Biol* 25:10261–10272.
10. Klein JA, et al. (2002) The harlequin mouse mutation downregulates apoptosis-inducing factor. *Nature* 419:367–374.
11. Pospisilik JA, et al. (2007) Targeted deletion of AIF decreases mitochondrial oxidative phosphorylation and protects from obesity and diabetes. *Cell* 131:476–491.
12. Vahsen N, et al. (2004) AIF deficiency compromises oxidative phosphorylation. *EMBO J* 23:4679–4689.
13. Ghezzi D, et al. (2010) Severe X-linked mitochondrial encephalomyopathy associated with a mutation in apoptosis-inducing factor. *Am J Hum Genet* 86:639–649.
14. Gabaldón T, Rainey D, Huynen MA (2005) Tracing the evolution of a large protein complex in the eukaryotes, NADH:ubiquinone oxidoreductase (Complex I). *J Mol Biol* 348:857–870.
15. Thorburn DR, et al. (2004) Biochemical and molecular diagnosis of mitochondrial respiratory chain disorders. *Biochim Biophys Acta* 1659:121–128.
16. Kruse SE, et al. (2008) Mice with mitochondrial complex I deficiency develop a fatal encephalomyopathy. *Cell Metab* 7:312–320.
17. Quintana A, Kruse SE, Kapur RP, Sanz E, Palmiter RD (2010) Complex I deficiency due to loss of Ndufs4 in the brain results in progressive encephalopathy resembling Leigh syndrome. *Proc Natl Acad Sci USA* 107:10996–11001.
18. Kirby DM, et al. (2004) NDUFS6 mutations are a novel cause of lethal neonatal mitochondrial complex I deficiency. *J Clin Invest* 114:837–845.
19. Spiegel R, et al. (2009) Mutated NDUFS6 is the cause of fatal neonatal lactic acidemia in Caucasus Jews. *Eur J Hum Genet* 17:1200–1203.
20. Stanford WL, Cohn JB, Cordes SP (2001) Gene-trap mutagenesis: Past, present and beyond. *Nat Rev Genet* 2:756–768.
21. Hansen GM, et al. (2008) Large-scale gene trapping in C57BL/6N mouse embryonic stem cells. *Genome Res* 18:1670–1679.
22. Barash Y, et al. (2010) Deciphering the splicing code. *Nature* 465:53–59.
23. Yang H, et al. (2010) Analysis of mouse models of cytochrome c oxidase deficiency owing to mutations in Sco2. *Hum Mol Genet* 19:170–180.
24. Wenz T, Diaz F, Spiegelman BM, Moraes CT (2008) Activation of the PPAR/PGC-1alpha pathway prevents a bioenergetic deficit and effectively improves a mitochondrial myopathy phenotype. *Cell Metab* 8:249–256.
25. Du XJ (2004) Gender modulates cardiac phenotype development in genetically modified mice. *Cardiovasc Res* 63:510–519.
26. Mattingly KA, et al. (2008) Estradiol stimulates transcription of nuclear respiratory factor-1 and increases mitochondrial biogenesis. *Mol Endocrinol* 22:609–622.
27. Li Y, et al. (2004) Androgen contributes to gender-related cardiac hypertrophy and fibrosis in mice lacking the gene encoding guanylyl cyclase-A. *Endocrinology* 145: 951–958.
28. Schiff M, Ogier de Baulny H, Lombès A (2011) Neonatal cardiomyopathies and metabolic crises due to oxidative phosphorylation defects. *Semin Fetal Neonatal Med* 16: 216–221.
29. Yen TY, et al. (2008) Acute metabolic decompensation and sudden death in Barth syndrome: Report of a family and a literature review. *Eur J Pediatr* 167:941–944.
30. Möller HE, et al. (2005) Magnetic resonance spectroscopy in patients with MELAS. *J Neurol Sci* 229–230:131–139.
31. Smolich JJ, Walker AM, Campbell GR, Adamson TM (1989) Left and right ventricular myocardial morphometry in fetal, neonatal, and adult sheep. *Am J Physiol* 257: H1–H9.
32. Einsiedel L, et al. (2010) Mitochondrial dysfunction in CD4+ lymphocytes from stavudine-treated HIV patients. *Mitochondrion* 10:534–539.
33. Pallotti F, Lenaz G (2001) Isolation and subfractionation of mitochondria from animal cells and tissue culture lines. *Methods Cell Biol* 65:1–35.
34. Anderson MF, Sims NR (2000) Improved recovery of highly enriched mitochondrial fractions from small brain tissue samples. *Brain Res Brain Res Protoc* 5:95–101.
35. Smith PK, et al. (1985) Measurement of protein using bicinchoninic acid. *Anal Biochem* 150:76–85.
36. Calvo SE, et al. (2010) High-throughput, pooled sequencing identifies mutations in NUBPL and FOXRED1 in human complex I deficiency. *Nat Genet* 42:851–858.
37. McKenzie M, Lazarou M, Thorburn DR, Ryan MT (2007) Analysis of mitochondrial subunit assembly into respiratory chain complexes using Blue Native polyacrylamide gel electrophoresis. *Anal Biochem* 364:128–137.
38. Morten KJ, Ackrell BA, Melov S (2006) Mitochondrial reactive oxygen species in mice lacking superoxide dismutase 2: Attenuation via antioxidant treatment. *J Biol Chem* 281:3354–3359.
39. Pepe S, McLennan PL (2002) Cardiac membrane fatty acid composition modulates myocardial oxygen consumption and postischemic recovery of contractile function. *Circulation* 105:2303–2308.